ORIGINAL CONTRIBUTION

A technical note on large normal-stress differences observed in a novel self-assembling functionalized dipeptide surfactant solution

Osama M. Maklad[1,2] · Kate McAulay[3,4] · Sandra Lerouge[5] · Dave J. Adams[3] · Robert J. Poole[1]

Abstract
A number of functionalised dipeptides self-assemble in water under specific conditions to give micellar aggregates. The micellar aggregates formed depend on the exact molecular structure and are important to understand as they control the properties both of the micellar phase and also of the gel phase which can be formed from these precursor solutions. Here, we investigate the rheological properties of a functionalised dipeptide which behaves as a surfactant at high pH. This solution has been shown previously to exhibit very "stringy" behaviour, and this has previously been characterised using capillary breakup extensional rheometry (CaBER). In the current technical note, we extend the rheological characterisation of an exemplar precursor solution via small-amplitude oscillatory shear and steady shear. Using a cone-and-plate geometry and a dedicated protocol, we can measure the first normal-stress difference N_1 and using a parallel-plate geometry to also measure (N_1-N_2), subsequently determining the second normal-stress difference N_2. In so doing, we confirm that these systems are highly elastic, e.g. for shear rates greater than ~ 30 s^{-1}, corresponding to a Weissenberg number based on the longest relaxation time ~ 330, $N_1 > 10\tau$ where τ is the shear stress, and also, we find that N_2 can be significant, is negative and approximately equal in magnitude to $\sim 0.36 \pm 0.05$ N_1. Significant uncertainties associated with the normal-stress difference data led to us using a range of different rheometers (and geometries) and highlight the issues with determining N_2 using this two-measurement approach. Despite these uncertainties, the non-negligible value of the second-normal stress difference is demonstrated for these fluids.

Keywords Micellar fluids · Dipeptide solutions · Normal-stress differences · Rheological characterisation

Introduction

A number of dipeptides functionalised with large hydrophobic aromatic groups can self-assemble in water (Du et al. 2015). The structures formed depend on the exact

✉ Robert J. Poole
robpoole@liv.ac.uk

1 School of Engineering, University of Liverpool, Liverpool L69 3GH, UK

2 School of Engineering, University of Greenwich, Kent ME4 4TB, UK

3 School of Chemistry, University of Glasgow, Glasgow G12 8QQ, UK

4 Department of Applied Science, School of Computing, Engineering and Built Environment, Glasgow Caledonian University, Glasgow G4 0BA, UK

5 Laboratoire Matière et Systèmes Complexes, Université de Paris Cité, Paris 75013, France

chemical structure and the pH of the water. There is significant interest in these materials as they form solutions with non-trivial rheological behaviour as well as the potential to form gels when salts are added or a pH change is carried out.

In the solution phase, the more hydrophobic examples form viscous solutions and have been shown to contain wormlike micelles (Chen et al. 2013; McAulay et al. 2020). A typical example is solutions of naphthalene-dipeptides 2NapFF (2NapFF = 2-(naphthalen-2-yl)-acetamido)-3-phenylpropanamido)-3-phenylpropanoic acid) (Fig. 1). At a pH of around 10.5 and a concentration of 0.1 wt%, 2NapFF forms anisotropic structures, whose morphology depends on the cation of the metal hydroxide used to form the high pH solution (McAulay et al. 2020). When caesium hydroxide is used, wormlike micelles are formed that are around 4.6 nm in diameter and microns in length (McAulay et al. 2020). Wormlike micellar formation can be shown by microscopy as well as small-angle neutron scattering (McAulay et al. 2020). These solutions show a highly elastic

Fig. 1 **a** Chemical structure of the caesium salt of 2NapFF; **b** cryo-TEM image of wormlike micelles formed by the caesium salt of 2NapFF at high pH; **c** small-angle scattering data (open circles) for the solution of the caesium salt of 2NapFF at high pH. The red line shows a fit to a flexible cylinder model, which is consistent with wormlike micelle formation. **b**, **c** are reproduced from McAulay et al., Chem. Commun., 2020, 56, 4094–4097 with permission from the Royal Society of Chemistry
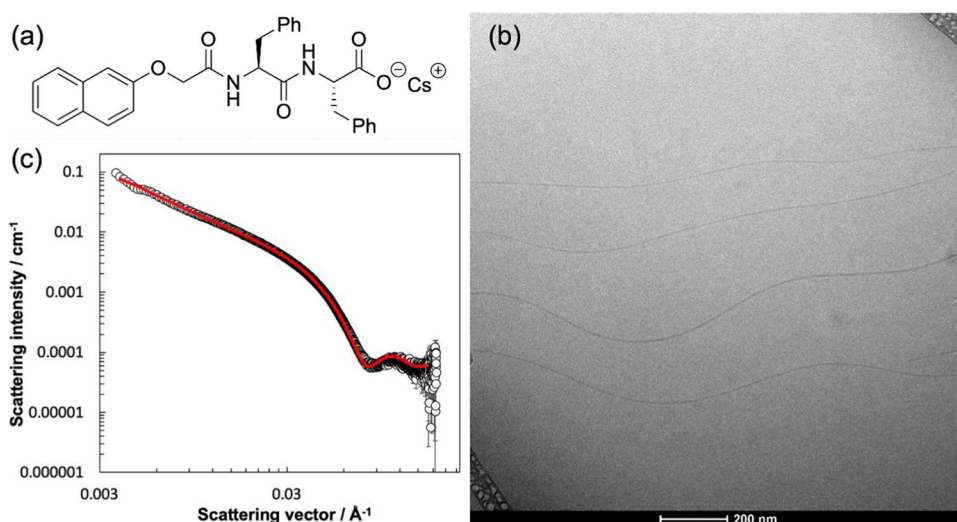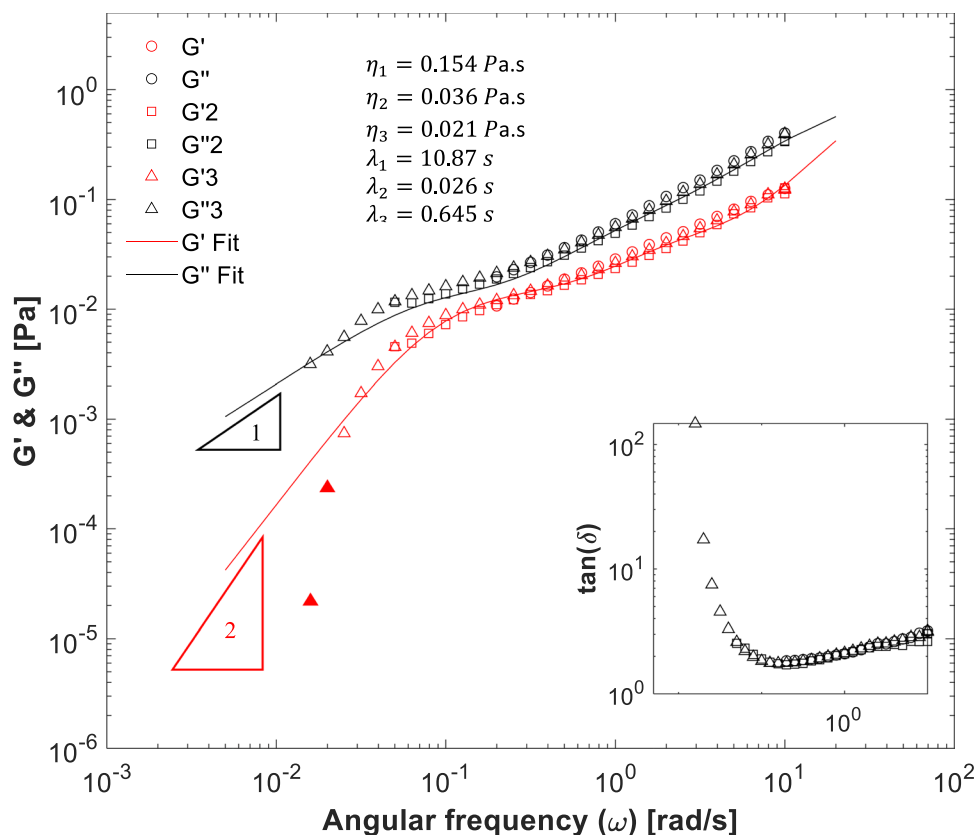

nature and exhibit significant extensional viscosity effects (e.g., relaxation times measurable using a capillary break up extensional rheometer (CaBER)). Although not seen in the cryo-TEM (Fig. 1b) due to the preparation processes involved in the technique, the shear viscosity and extensional viscosity appear to arise from entanglements; no evidence for permanent cross-links is found in the microscopy and neither is there any evidence of branching (see, e.g. the cryo-TEM data in Fig. 2 of McAulay et al., 2020). Although the cryoTEM data does not show entanglements, it exemplifies the presence of these micellar structures, agreeing well with the fits to the small-angle scattering data (which probes the bulk) for example, confirming that these systems are wormlike micelles.

These solutions show interesting behaviour. Addition of calcium or magnesium salt at high pH results in gel

Fig. 2 Small-amplitude oscillatory shear (SAOS) conducted at a fixed oscillation stress of 0.1 Pa for 2NapFFCs with a three-mode Maxwell fit (solid lines) and values of fitting parameters in the inset. Terminal behaviour is observed at low frequencies where the expected quadratic behaviour ($\sim \omega^2$) for the storage modulus and linear response for the loss modulus ($\sim \omega$) is seen. The two solid red triangles at low frequency are not included in the fit of G'. Repeat measurements indicated by different symbols. Inset shows tan δ

$\eta_1 = 0.154\ Pa.s$
$\eta_2 = 0.036\ Pa.s$
$\eta_3 = 0.021\ Pa.s$
$\lambda_1 = 10.87\ s$
$\lambda_2 = 0.026\ s$
$\lambda_3 = 0.645\ s$

formation (Chen et al. 2013). Gels are also formed if the pH is decreased. In the micellar phase, heating and cooling the solution results in a significant increase in the extensional viscosity, which is due to a change in the molecular packing in the micellar aggregates resulting in more rigid structures being formed (Draper et al. 2017a, b). It is also possible to align the micellar aggregates using a magnetic field (McAulay et al. 2020). Outside of steady shear viscosity and CaBER data, the broader rheological response of these dipeptide solutions has yet to be investigated, and the purpose of the current paper is to address this topic, with emphasis on non-linear normal stresses developed during steady shear. Of particular interest is how the rheology of these novel, apparently wormlike, micellar fluids compares to those more classic, wormlike micellar solutions formed by the self-assembly of surfactants in solution (Rehage and Hoffmann 1991). Such wormlike micelles or "living polymers" — so-called due to their rheological response being similar in many ways to polymer solutions (Fardin and Lerouge 2014) — are of particular interest from a rheological perspective because their long flexible cylindrical geometry can lead to entanglement even at relatively low concentrations (Rehage and Hoffmann 1991). In semi-dilute solution, these wormlike micelles exhibit remarkably simple rheological behaviour; their linear rheology measured in small amplitude oscillatory shear flow is often well described by a single-element Maxwell model with a single relaxation time (Berret 2006). The non-linear rheological and flow response of wormlike micelles has proven to be incredibly rich both in simple shear flow (Lerouge and Berret 2009) and in more complex flow configurations combining shear and extensional deformation (see Rothstein and Mohammadigoushki 2020). In the semi-dilute concentration range, wormlike micelles can display simple shear thinning (in the low limit of this concentration range), but the prevailing behaviour is to exhibit so-called shear-banding flow. In the latter case, the fluid exhibits a non-monotonic constitutive curve (i.e. the shear stress vs shear rate curve enforcing the homogeneity of the flow). Experimentally, the corresponding flow curve presents a stress plateau above a critical shear rate, and the flow splits into domains bearing high and low shear rates (Divoux et al. 2016). The dipeptide wormlike micellar solutions used here do not appear to exhibit such shear banding but simple shear thinning. Although there have been many papers reporting shear rheology data for classical wormlike micelles (see, e.g. the review of Anderson et al. 2006), there has been surprisingly little measurements of the normal-stress differences. A few measurements of normal-stress differences are available in the dilute regime where the systems exhibit shear thickening (Lee et al. 2002) and in the concentrated regime where shear banding is also observed (Helgeson et al. 2009). In the semi-dilute regime, it appears that most normal stress data in the literature,

starting with a single plot of the transient behaviour of N_1 at a single shear rate in the seminal work of Rehage and Hoffmann (1988) is for systems based on cetylpyridinium chloride (CPyCl) and sodium salicylate (NaSal) at various concentrations. Steady-state data across a broad range of shear rates for both a CPyCl/NaSal system and a system based on cetrimonium bromide (CTAB) and sodium salicylate ("CTAB-NaSal") (Fischer and Rehage 1997) show that the CPyCl/NaSal system exhibits classical quadratic scaling of N_1 with shear rates at low shear rates (with N_1/τ reaching a maximum ~ 3); beyond this shear rate, it is likely the data shown are not at steady-state (see, e.g. the SI data in López-Barrón et al. (2014) where N_1 is seen to increase in the whole shear-banding regime). In contrast, the CTAB/NaSal system has no N_1 data at low shear rates but at higher rates appears to scale approximately linearly with shear rate. There is a concomitant shear-thinning of the viscosity in this range (the shear stress scaling approximately as $\tau \propto \dot{\gamma}^{0.25}$) which enables N_1/τ to reach very high values (~ 30 at the highest shear rate of $\sim 50 \, \text{s}^{-1}$ corresponding to a Weissenberg number of 35 based on a small amplitude oscillatory shear relaxation time (0.7 s)). Similarly, large values of the maximum of N_1/τ have also been observed for a range of CPyCl/NaSal systems (Pipe et al. 2010; Vilageliu 2013), CTAB/NaNO$_3$ (Fardin and Lerouge, 2012) and a system based on cetyltrimethylammonium tosylate ("CTAT") (García-Sandoval et al. 2018). Only one study seems to have measured N_2 directly for a semi-dilute entangled wormlike micellar fluid; Pipe et al. (2010), using a cone-and-plate geometry combined with a measurement of the pressure gradient (Baek and Magda 2003), found $-\frac{N_2}{N_1} \sim 0.4$ for a CPyCl/NaSal system but with significant uncertainty as the data is susceptible to small variations in the fitted slope (we note there are also limited N_2 data in the Ph.D. thesis of Ober 2013). A few datasets have also been reported regarding the transient response of N_1 following step shear rate in CPyCL/NaSal solutions (Fischer and Rehage 1997; Gaudino et al. 2020). Finally, Kim et al. (2013) used a superposition of an oscillatory motion onto a steady-state shear flow to probe a semi-dilute wormlike micellar solution based on CPyCl/NaSal/NaCl. In this case, the values for the normal stress components can also be obtained directly, without complex fitting procedures, from the in-phase superposition moduli. The data is consistent with a Giesekus model (Giesekus 1982) such that $-\frac{N_2}{N_1} \sim 0.25$ in the low shear rate range. Thus, the limited data available for semi-dilute wormlike micelles would suggest that N_2 is not negligible for such systems and at least as important as it is in concentrated and entangled polymeric solutions (see the data reviewed in Maklad and Poole 2021).

In the current paper, we investigate the shear rheology of one such functionalised dipeptide solution ("2NapFF"),

which we have previously shown exhibits strong extensional viscosity effects with particular attention placed on steady shear flow and the normal-stress differences developed under flow.

Working fluids

The sample preparation and chemical characterisation of the so-called 2NapFF functionalised dipeptide solutions used in the current study were previously reported in Draper et al. (2017a, b). 2NapFF consists of two amino acids connected by a peptide bond which are functionalised at the N-terminus by two naphthalene aromatic groups. 2NapFF solutions form low-molecular–weight hydrogels (LMWGs) when the pH is decreased. In the "precursor" phase (i.e. prior to gelation caused by pH decrease), 2NapFF self-assembles and forms wormlike micellar structures (Chen et al. 2010; Draper et al. 2020). Here, we study a single concentration of 10 mg mL^{-1} in aqueous solution. Controlling the sample preparation methodology is critical for ensuring reproducibility. To prepare the working fluids, the terminal carboxylic acid was deprotonated using caesium hydroxide (CsOH). The salt addition deprotonates the carboxylic acid, resulting in a surfactant-like structure and exhibiting very "stringy" behaviour which was found to correlate with relaxation times on the order of 1 s using capillary breakup extensional rheometry (CaBER) (Draper et al. 2017a, b). To prepare the solutions, 1 molar equivalent of caesium hydroxide was added using a 0.1 M solution with respect to 2NapFF and then deionised water added to make up the final volume to give a concentration of 2NapFF of 10 mg mL^{-1}. Seventeen millilitres of the 2NapFF solution was prepared in 50-mL Falcon tubes, stirred with a 25×8-mm stirrer bar and wrapped in Parafilm. The sample was stirred at 1000 rpm for 7 days and then left to stand before measurement. All solutions were formed at room temperature (normally between 22 and 25 °C).

Experimental methods

We characterised the rheology of our functionalised dipeptide solution in small amplitude oscillatory shear (SAOS) and steady shear using both cone-and-plate and parallel-plate devices to allow us to obtain both the first and second normal-stress differences.

Small amplitude oscillatory shear (SAOS) measurements were performed using a TA instruments AR 1000 N controlled-stress rheometer. To minimise inertial effects, a light-weight 6-cm-diameter 2° acrylic cone was used at an operating temperature 20 °C, which was controlled by a Peltier plate with precision within ± 0.1 °C, and, to prevent

evaporation, a solvent trap was employed. A stress sweep was performed at a frequency of 1 rad/s to determine the linear viscoelastic (LVE) regime for oscillation stresses ranging from 0.01 to 20 Pa. The oscillation stress chosen in the LVE range to perform the frequency sweep tests was 0.1 Pa over three decades of frequency from 0.01 to 10 rad/s.

Steady shear tests to determine both first and second normal-stress differences were performed on two different stress-controlled Anton Paar MCR 302 rheometers. A 1° steel cone-and-plate geometry with either 5 or 6 cm diameter (CP50 and CP60 respectively) was used to measure the first normal-stress difference N_1 and, using a 5-cm diameter parallel-plate geometry (PP50) made from steel, at a gap of 0.5 mm, to measure $N_1 - N_2$ through the measurement of the axial thrust using the following two equations:

$$N_1(\dot{\gamma}) = \frac{2F_{CP}(\dot{\gamma})}{\pi R^2} \tag{1}$$

$$N_1(\dot{\gamma}) - N_2(\dot{\gamma}_R) = \frac{2F_{PP}(\dot{\gamma}_R)}{\pi R^2}\left(1 + \frac{1}{2}\frac{dlnF_{pp}(\dot{\gamma}_R)}{dln\dot{\gamma}_R}\right) \tag{2}$$

where F_{CP} is the axial thrust from the cone-and-plate geometry $\dot{\gamma}$, is the shear rate (and $\dot{\gamma}_R$ is the shear rate at the "rim" or edge of the parallel plate), R is the radius of the geometry in use, and F_{PP} is the axial thrust from the plate-and-plate geometry.

All steady shear measurements were performed at a fixed temperature of 20 °C, which was controlled using a Peltier plate with precision of ± 0.01 °C, and, to prevent evaporation, a trap was again used. The measurements were realized through two different approaches, the first one used a dedicated protocol (protocol no. 1) (Casanellas et al. 2016; Poole 2016), with 13 different shear "peak hold" intervals being applied to the sample for 300 s for each shear rate in the following order (0.01–10-0.01–20-0.01–50-0.01–100-0.01–200-0.01–500-0.01 s^{-1}). This protocol is essentially a series of "start-up" experiments that enable us to determine the steady state for each shear rate. The only difference to standard start-up experiments is that after each shear rate, we do a "baseline" repeat of our lowest shear rate (0.01 s^{-1}) to allow us to account for normal-force drift. The repeated low shear rate value between each step, where the normal-stresses should be negligible as they must scale as the square of the shear rate in this limit (Barnes et al. 1989), then allows us to empirically correct for the normal-force transducer drift that was observed with the cone-and-plate geometry. This drift was fit to a linear fit through the low shear rate datasets immediately before and after each high shear interval, and then, this fit was used to "add on" the corresponding value to correct the data such that $N_1 = 0$ identically for each low shear rate interval. An example of

this uncorrected data is shown in Fig. 6 in Appendix 1 with the linear fit for the low shear rate values shown as a dashed line for one of the intervals at 200 s^{-1}. Moreover, to correct for inertia effects, Eq. 3 was used to add an amount (ΔF) to the normal force measurement (Barnes et al. 1989):

$$\Delta F = \frac{3}{40}\pi\rho\omega^2 R^4 \tag{3}$$

where ρ is the fluid density, ω is the angular frequency of the rotation, and R is still the radius of the geometry used. After corrections for both the normal force transducer drift and inertia, the last 30 measurement points were averaged to compute the viscosity and normal-stress differences at each corresponding shear rate.

The second protocol (protocol no. 2) used was the application of a logarithmic decreasing rate sweep to a fresh sample, starting from 500 s^{-1} down to 0.005 s^{-1}, with a sampling time of 60 s per data point and a resolution of 10 pts/decade. For the smallest applied shear rates, typically between 0.005 and 1 s^{-1}, the thrust was found to be approximately constant but nonzero. For each flow geometry (PP and CP), the value of the thrust averaged over this small range of low shear rates was subtracted from the whole set of data points to correct the measured thrust as a function of the shear rate. The inertia correction (Eq. 3) was then applied to the dataset.

Results and discussion

Small amplitude oscillatory shear results

Figure 2 shows SAOS experimental data for the functional dipeptide solution along with "Maxwell" fits for G' and G'', represented by the solid lines, which correspond to a three-mode fit:

$$G' = \frac{\eta_1.\lambda_1.\omega^2}{1+\left(\lambda_1.\omega\right)^2} + \frac{\eta_2.\lambda_2.\omega^2}{1+\left(\lambda_2.\omega\right)^2} + \frac{\eta_3.\lambda_3.\omega^2}{1+\left(\lambda_3.\omega\right)^2} \tag{4}$$

$$G'' = \frac{\eta_1.\omega}{1+\left(\lambda_1.\omega\right)^2} + \frac{\eta_2.\omega}{1+\left(\lambda_2.\omega\right)^2} + \frac{\eta_3.\omega}{1+\left(\lambda_3.\omega\right)^2} \tag{5}$$

where G' is the storage modulus (Pa), η_i is the ith polymeric viscosity component (Pa s), λ_i is the ith mode relaxation time (s), ω is the angular frequency (rad/s), and G'' is the loss modulus (Pa). (NB. Increasing the number of modes to four makes a negligible decrease in the error and does not alter either the estimate of the longest relaxation time (10.94 s cf 10.87 s) or the mode-averaged relaxation time). Three repeat datasets are included in Fig. 2 to highlight consistency. The values of each of these parameters are included as an inset in Fig. 2 and in Table 1. At low frequencies, G' varies

Table 1 Maxwell mode fitting parameters

Viscosity modes			Relaxation times		
η_1(Pa.s)	η_2(Pas)	η_3(Pas)	λ_1(s)	λ_2(s)	λ_3(s)
0.154	0.036	0.021	10.87	0.026	0.645

quadratically, and G'' varies linearly with frequency showing the expected terminal behaviour (Barnes et al. 1989) although the smallest G' values, highlighted by the use of filled symbols in Fig. 2, are close to the resolution of the instrument and were therefore not included in the fit. We note that the shape of the G', G'' curves are very different from the single-mode Maxwell behaviour usually observed in classical wormlike micelle systems in the semi-dilute regime (López-Barrón et al. 2014). For such classical systems, as they are so well fit by a single-mode model, the cross-over frequency where $G' = G''$ can be used directly to determine the relaxation time (via the reciprocal of the cross-over frequency). In contrast, for the functionalised dipeptide solution used here, there is no strict cross over frequency as the storage modulus remains lower than the loss modulus across the whole frequency range (although the datasets are closest at a frequency ~ 0.2 rad/s). Additionally, there is a clear minimum in the magnitude of tan (δ), which also occurs at 0.2 rad/s. We note that Oelschlaeger et al. (2009) measure G' and G'' on CPyCl/NaSal systems as a function of ω over a very large range of angular frequencies using diffusing wave spectroscopy, at various temperatures, and the data exhibits some similarities with our system.

Shear viscosity and normal-stress difference results

Figure 3a and b show the measurements of the shear viscosity, first normal-stress difference N_1 and the difference between normal stresses (N_1-N_2) using CP60 and PP50 geometries respectively and protocol no. 1. The shear viscosity measurements are in good agreement between both geometries; however, the first normal-stress difference for the cone-and-plate geometry was affected by normal force transducer drift which was not observed in the parallel-plate geometry, as shown in Fig. 6 in Appendix 1. As already discussed, this normal force drift was corrected using the method described in "Experimental methods." It can be immediately seen that the N_1-N_2 data are noticeably higher than the N_1 data indicating that N_2 is negative and non-negligible for these fluids.

The sensitivity of the results to the chosen geometry was also checked, and some limited measurements were conducted with a smaller 4-cm diameter 1° acrylic cone-and-plate geometry, as shown in Fig. 7 in Appendix 2, and via varying the gap for the parallel-plate geometry as shown
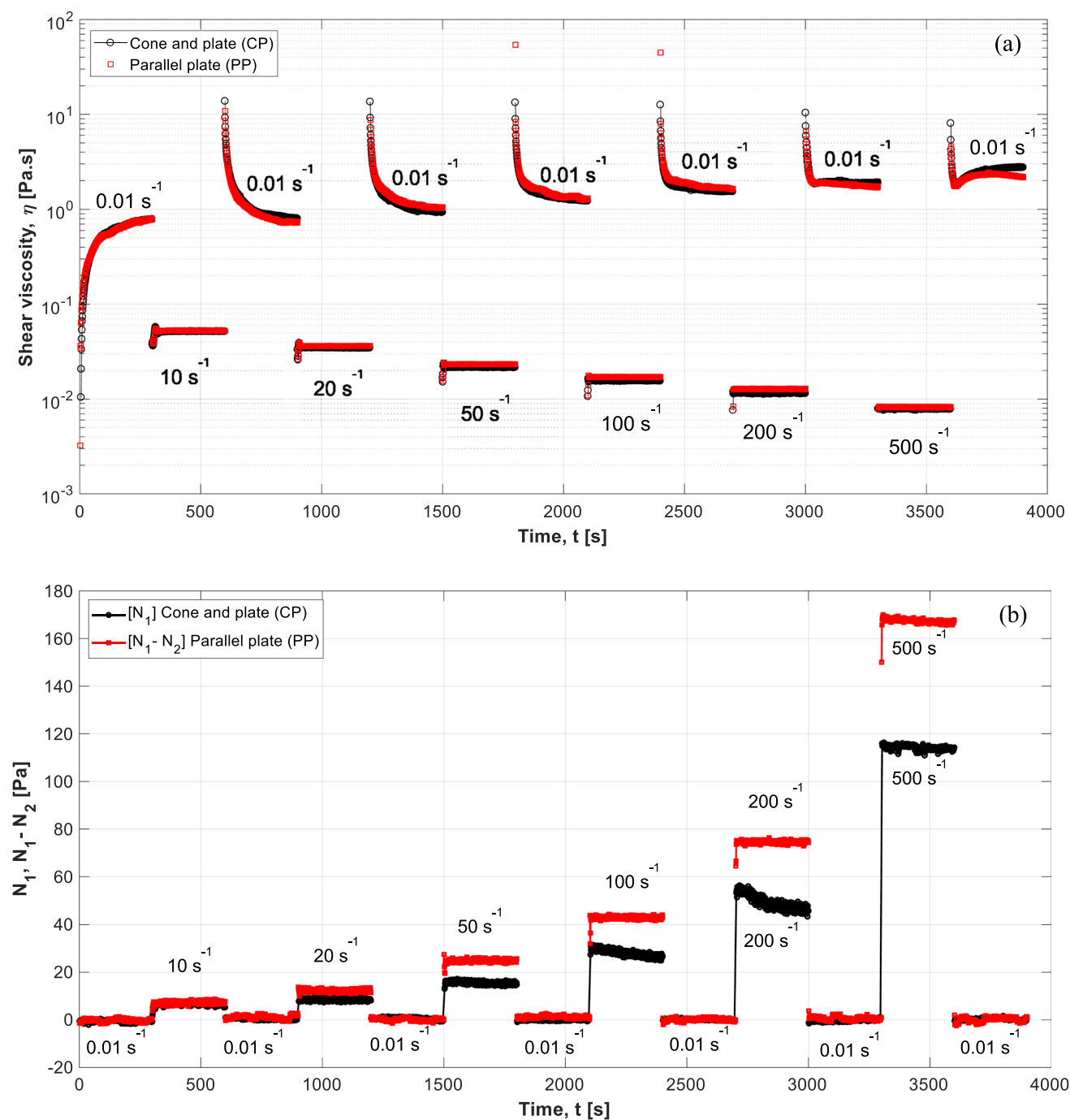
Fig. 3 (**a**) Shear viscosity and (**b**) and normal-stress differences against time for various peak hold shear rates (indicated in figure) for 2NapFF-Cs solution using cone-and-plate and parallel-pate geometries. Normal force transducer drift and inertia have been corrected for normal-stress difference data (protocol and original data shown in Appendix 1 Fig. 6

in Fig. 8 also in Appendix 2. These checks were undertaken given the surprisingly large values of N_2 observed in order to confirm repeatability of the result (and check sensitivity). Good agreement between the datasets was observed with these geometric variations giving confidence in the results and also suggesting slip is not an issue for these systems.

Figure 4 shows the shear viscosity (η) (Fig. 4a), first normal-stress difference (N_1) (Fig. 4b), and the difference between first and second normal-stress differences (N_1-N_2) (Fig. 4c), as a function of the shear rate as obtained by averaging the last 30 points of the data shown in Fig. 4. Additionally, all figures contain additional data using protocol
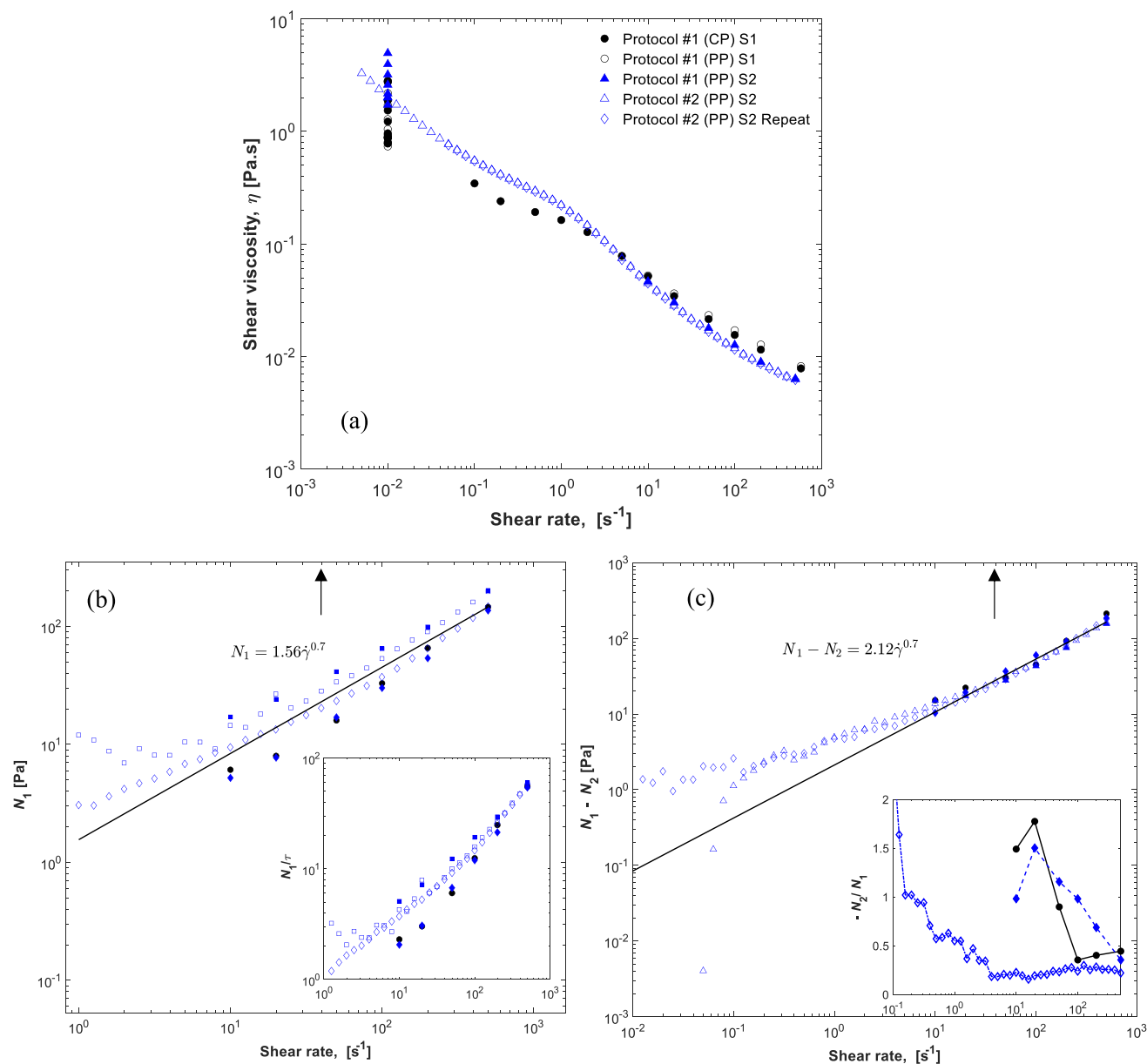
Fig. 4 **a** Time average shear viscosity data and **b**, **c** normal-stress differences data against shear rate from both peak hold and rate sweep protocols; black symbols are for measurements using protocol no. 1, and blue symbols for protocol no. 2 both using MCR302 (for protocol no. 1 averages determined via the last 30 s of the shear interval data shown in Fig. 3). Inset in b shows the ratio between first normal-stress difference and shear stress against shear rate. Table 2 lists fitting parameters

no. 2 (obtained on a separate rheometer and by a different user). The repeatability of the data across protocols and samples is generally good, especially for viscosity and the parallel-plate normal force (i.e., N_1-N_2) at higher shear rates. The effect of shear history is most easily seen in the viscosity data: protocol no. 2, which goes from high to low shear rates, gives higher viscosities for shear rates less than 1 s^{-1}. The broad spread of viscosity data at the lowest shear rate (0.01 s^{-1}) — with each data point corresponding to a different shear history with each return to the "baseline"

in protocol no. 1 — also highlights the sensitivity to prior shearing. Differences in creating nominally identical samples — as highlighted earlier — may also be responsible for some of the differences observed between the results across protocols. We also note that despite the high level of elasticity measured both in SAOS and in steady shear, the data do not exhibit any signs of flow instability (i.e. due to inertia or elasticity), and any fluctuations around the steady state values generally remained less than 1%. Some in situ measurements of structure across these shear rate range would be

of interest to determine if shear-induced viscosity changes correlate with a change in the microstructure, but this is outside the scope of the current study.

As the previous CaBER data suggested, our normal-stress data confirms that these dipeptide systems are highly elastic. For example, the ratio of N_1 to τ (where τ is the shear stress) is often taken as a measure of how elastic a liquid is: specifically, $N_1 > 2\tau$ is used and is called the "recoverable shear" (Barnes et al. 1989). One can also think of this as a Weissenberg number based on the ratio of elastic to viscous stresses (Morozov and van Saarloos 2007; Poole 2012). For the dipeptide solutions and for shear rates greater than about 30 s^{-1}, corresponding to a Weissenberg number based on longest relaxation time ~ 330, we see that $N_1 > 10\tau$. In addition, we find that N_2 is significant, negative and equal in magnitude to ~ 0.36 ± 0.05 N_1. To obtain these shear-rate independent estimates, we forced all the normal force data to be identical power-law functions of shear rate (in this case, forcing the best fit for a power-law value of 0.7). Complete fit information is given in Table 2. This ratio of N_2 to N_1 is broadly consistent with the only known N_2 results for a classical semi-dilute entangled wormlike solution based on cetylpyridinium chloride (CPyCl) and sodium salicylate (NaSal) (Pipe et al. 2010; Ober 2013).

Given the known difficulties of using this approach to estimate N_2, and in order to double check the normal-stress difference results, measurements were taken on different rheometers and by different users in both Liverpool and Paris (using different protocols). There was some scatter in the measurements, but overall the data is in broad agreement. In particular, the scatter of the N_1 data (from the cone-and-plate geometry) is higher than the data for N_1-N_2 (from the parallel-plate geometry) which is consistent with the data in Appendix 1 Fig 6 where the cone-and-plate suffers from significant zero-shear rate "drift" issues which are absent from the corresponding parallel-plate data.

It is tempting to try to infer some microstructural information from the normal-stress data, especially with regard to the large N_2 observed for this system where for some experiments, it was seen that N_2 could approach N_1 in magnitude (i.e. $N_1 \sim$ -N_2). Such behaviour has been

predicted to occur theoretically for fluids exhibiting "sheet-like" or "film-fluid-like" behaviour (Larson 1997). In this paper, Larson (1997) shows that for certain film models, the predicted behaviour is precisely $N_1 = -N_2$ and offers the following explanation "Films, on the other hand, orient parallel to the XZ plane in shear so that both τ_{xx} and τ_{zz} are large compared to τ_{yy}. This implies that $N_2 \sim$ -N_1 for films.". Clearly, constitutive equations that can predict non-vanishing N_2 in steady simple shear, via incorporating either quadratic stress terms (such as the Giesekus model Giesekus 1982) or the full Gordon-Schowalter derivative, such as the Phan-Thien and Tanner (Phan-Thien and Tanner 1977) model for polymeric systems, may be required to accurately model these systems in steady shearing.

As is clear from Fig. 3a, these peptide solutions also exhibit some shear history effects as upon increasing the shear rate and returning to the same low shear rate; the shear viscosity at the low shear rate value of 0.01 s^{-1} can be seen to be continually increasing with each repetition (which is, of course, "sandwiched" between increasing shear rates altering the shear history experienced by the sample each time). This change in viscosity may be due to air bubbles being introduced via instability, or ejection of material; however, we do not believe this to be the case. If material was being ejected, then we would expect significantly lower viscosities when we do the baseline repeat after each step, and this is not what is observed. We believe the introduction of air bubbles causing this subtle shift is also unlikely. To avoid evaporation, we make use of a solvent trap which, for protocol no. 1 measurements, precludes a direct visual observation of what is happening, but the excellent repeatability of the datasets on the same sample would suggest air introduction via instability is unlikely. For protocol no. 2, we used a transparent solvent trap and did not observe any evidence of instability/air entrainment. The repeatability between experiments using cone-and-plate and parallel-plates shown in Fig. 3a is also excellent which is also inconsistent with the differences being driven by an instability rather than shear history. In Fig. 5a, the shear stress is plotted against shear rate highlighting this increase. To probe this shear history effect — and to determine if it is reversible given sufficient rest — Fig. 5b shows data with pre-shear at 1000 s^{-1} followed by a 1-h waiting time, and the viscosity increase at low rate appears to be permanent. However, in Fig. 5c, viscosities with and without a significant pre-shear, but otherwise following the same protocol (no. 1) as adopted for the earlier measurements, show there are subtle effects and that shearing at slightly higher rates seems to "reset" the dataset which had the pre-shear at 1000 s^{-1}. Small differences that emerge at higher rates may simply be due to repeatability issues or an indication of genuine differences in the rheology due to the different shear histories.

Table 2 Normal-stress data fits from both protocol no. 1 and protocol no. 2 and combined datasets

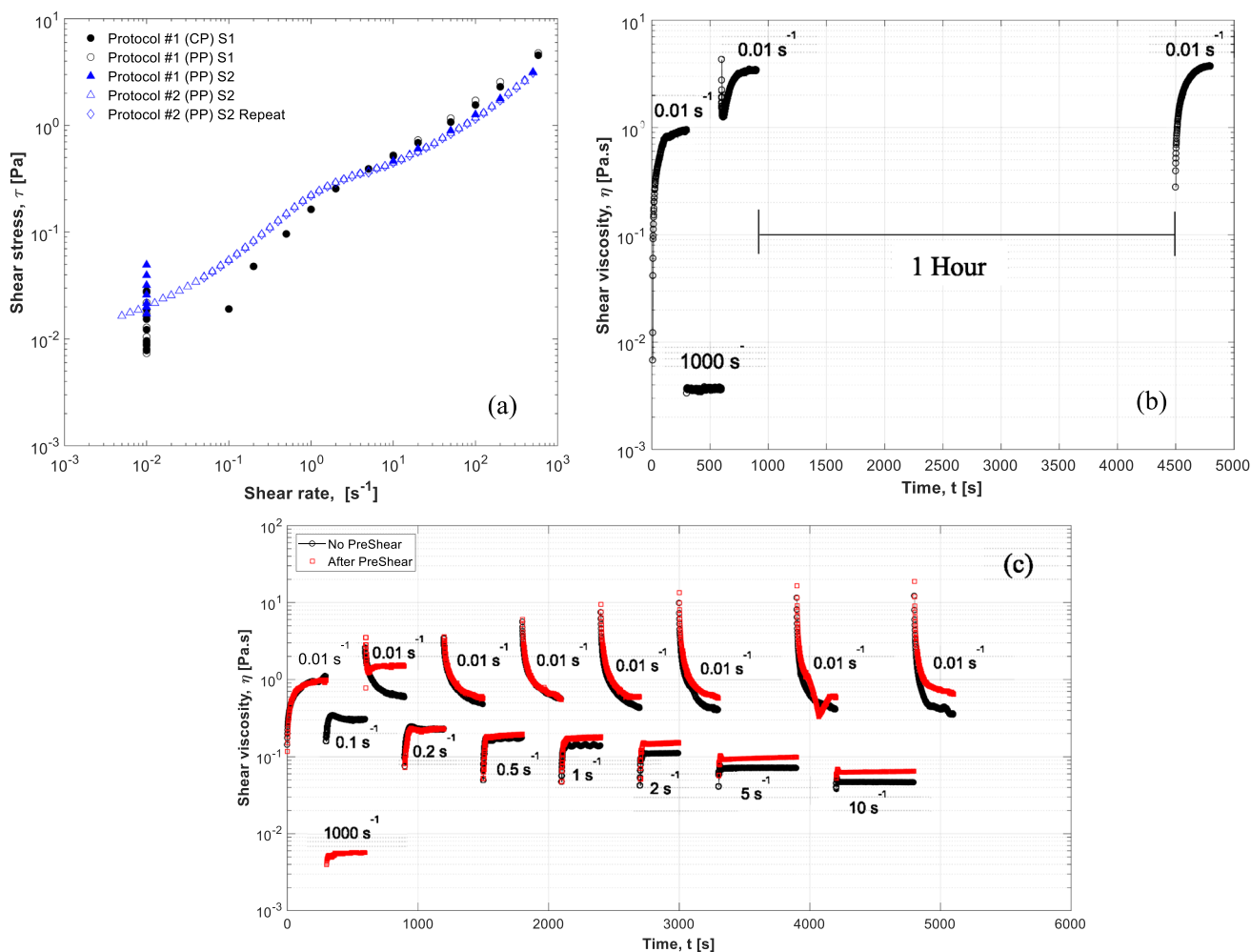|	Best fits individual data sets		Forced fits all data (same exponent)		
	N_1(Pa)	$N_1 - N_2$(Pa)	N_1(Pa)	$N_1 - N_2$(Pa)	$-N_2/N_1$
Protocol no. 1	$0.7\dot{\gamma}^{0.84}$	$2.86\dot{\gamma}^{0.66}$	$1.56\dot{\gamma}^{0.7}$	$2.02\dot{\gamma}^{0.7}$	0.36
Protocol no. 2	$0.67\dot{\gamma}^{0.84}$	$2.1\dot{\gamma}^{0.72}$			

Fig. 5 **a** Shear viscosity against shear stress where a pre-shear effect becomes apparent for 0.01 s^{-1} shear rate peak hold intervals (taken from Fig. 4a), **b** is a pre-shear test and 1-h waiting time, and **c** is peak hold protocol with a pre-shear interval at 1000 s^{-1}

Conclusions

We have studied the linear (SAOS) and non-linear (N_1, N_2) rheology of a novel functionalised dipeptide system which self-assembles in water under specific conditions to give entangled wormlike micellar aggregates. Although these solutions had previously been characterised via steady shear viscometry and transient uniaxial extension (using CaBER), their broader rheological characteristics had not been studied in detail. The SAOS linear rheology reveals significant differences to "classical" wormlike micellar systems (e.g. those based on CpyCl/NaSal for example) — which are usually very well fit by a single Maxwell mode — such that a cross-over point enables easy estimation of the longest relaxation time. For the non-linear shear rheology, the use of a cone-and-plate geometry and a dedicated protocol allowed us to measure the first normal-stress difference N_1. Following this, a parallel-plate geometry provides the difference between normal stress differences (N_1-N_2). Postprocessing the results allows the second normal-stress difference N_2 to then be determined. In so doing, we confirm that these systems are highly elastic, e.g. for shear rates greater than ~ 30 s^{-1}, corresponding to a Weissenberg number based on longest relaxation time ~ 330, the first normal stress difference $N_1 > 10\tau$ where τ is the applied shear stress. We also find that N_2 can be significant, is negative and is approximately equal in magnitude to ~ 0.36 ± 0.05 N_1. Significant uncertainties associated with the normal-stress difference data led to us using a range of different rheometers (and geometries) to confirm this result whilst highlighting the known issues with determining N_2 using this two-measurement approach. Despite these uncertainties, the non-negligible value of the second-normal stress difference is demonstrated for these fluids.
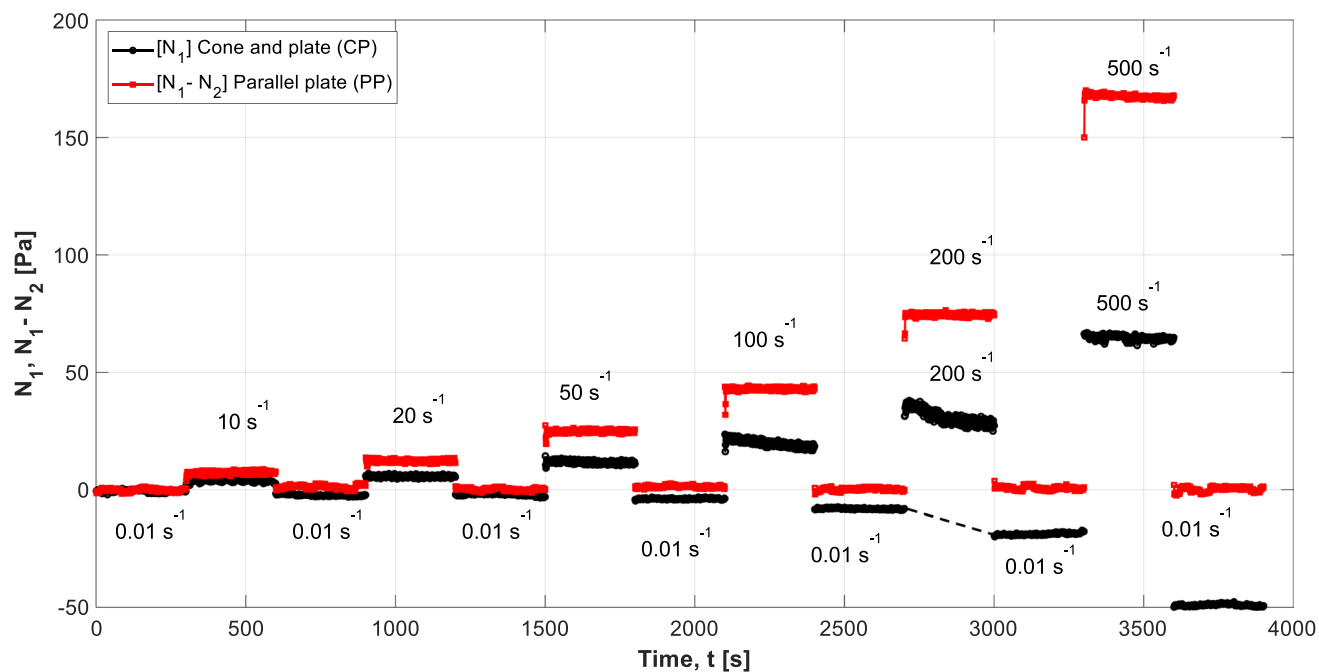
Appendix 1

Fig. 6 Normal-stress differences against time for 2NapFF-Cs solution using cone-and-plate and parallel-plate geometries (data corrected for inertia). Normal force transducer drift was observed for N_1 using cone-and-plate geometry. The dashed line is linear fit for the low shear rate values shown for the shear interval at $(200 s^{-1})$
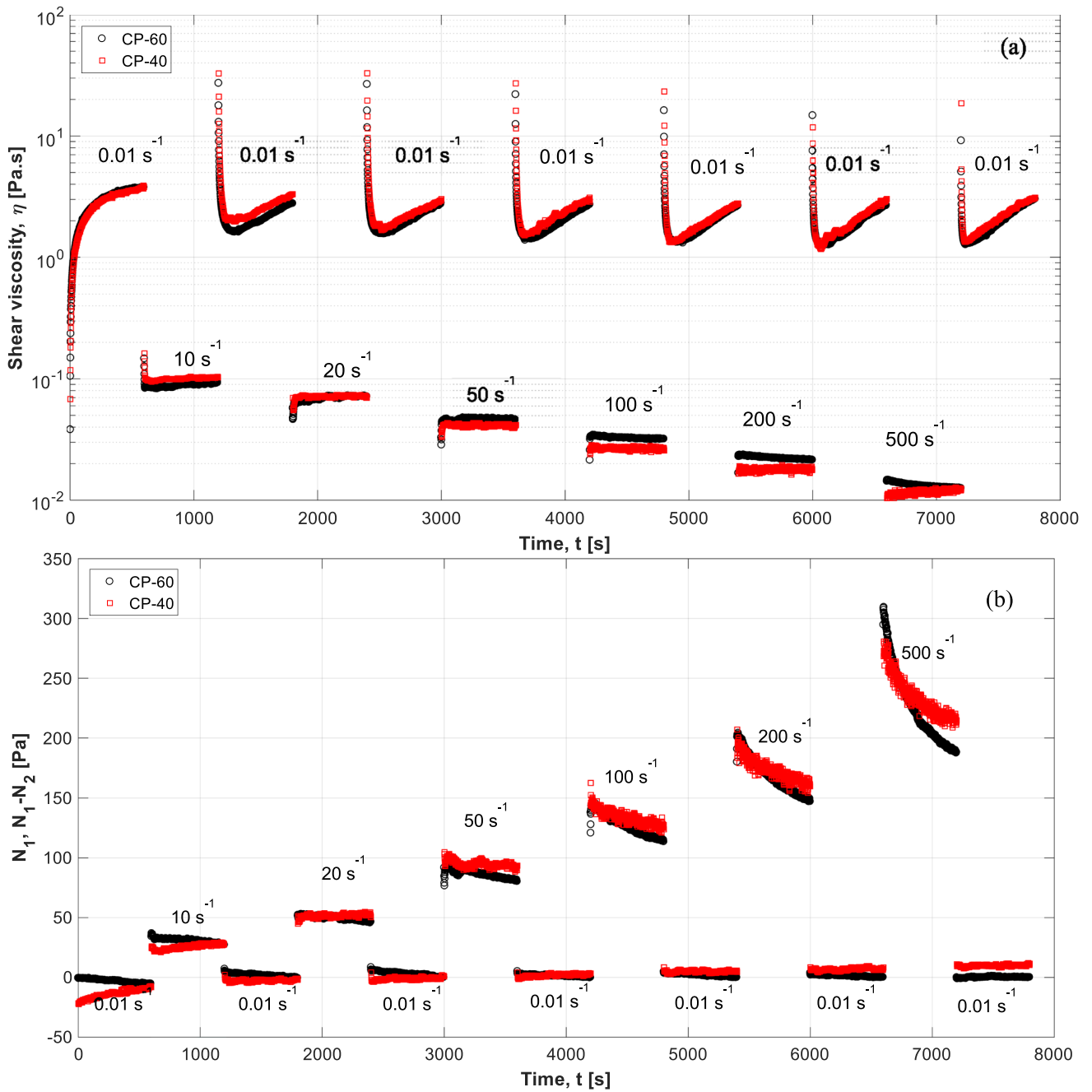
Appendix 2

Fig. 7 Shear viscosity in (**a**) and normal-stress differences in (**b**) against time for 2NapFF-Cs solution using cone-and-plate and parallel-pate geometries. Normal force transducer drift and inertia have been corrected for N_1 from CP-60- and CP-40
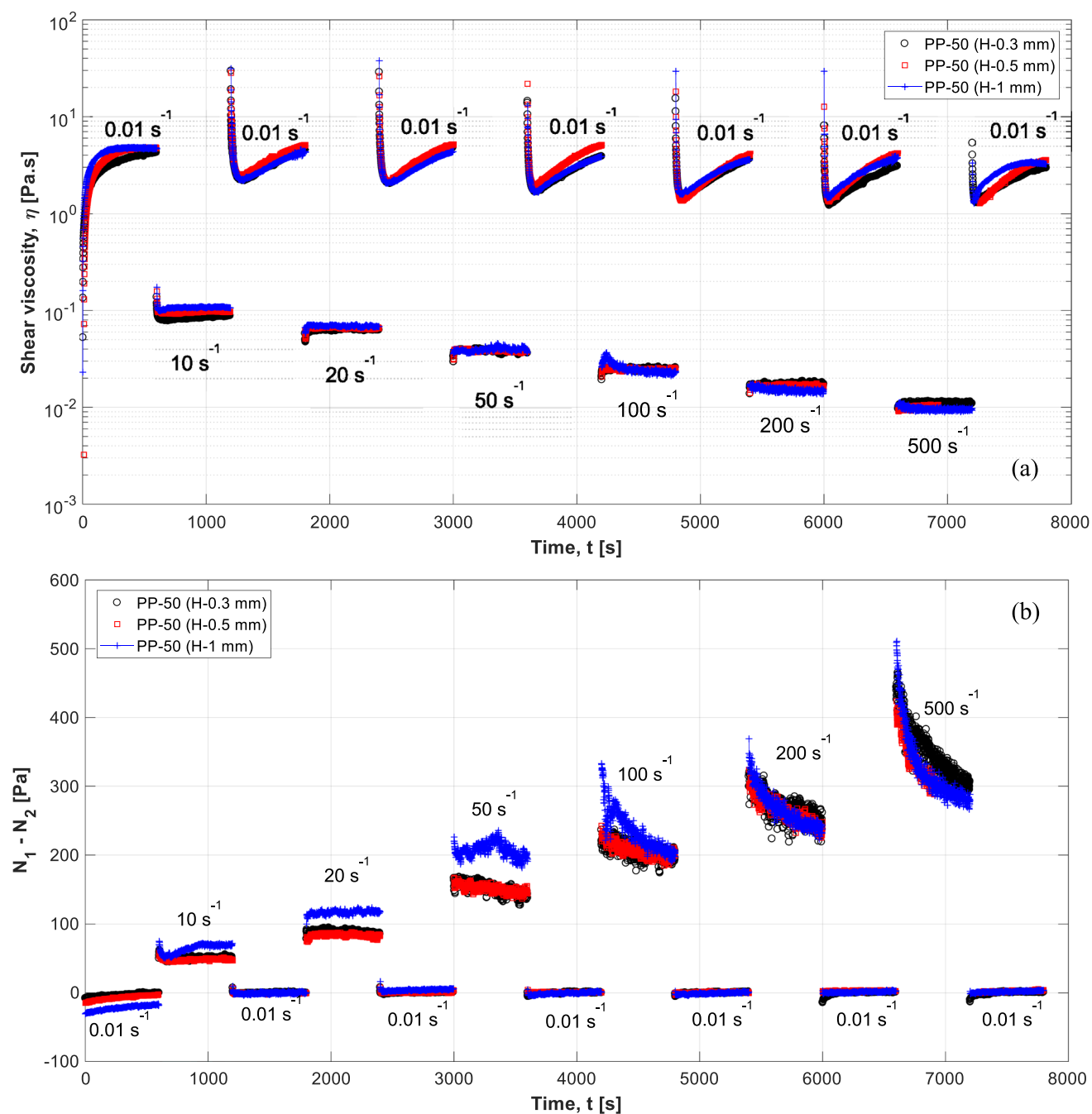
Fig. 8 Shear viscosity in (**a**) and normal-stress differences in (**b**) against time for 2NapFF-Cs solution using parallel-pate geometry at three different gaps 0.3, 0.5, and 1 mm. Data shows good repeatability across all three gaps for shear viscosity and for normal-stress difference at the two largest gaps

Declarations

Competing interests The authors declare no competing interests.

References

Anderson VJ, Pearson JRA, Boek ES (2006) The rheology of worm-like micellar fluids. Rheol Rev 2006:217–253. http://www.bsr.org.uk. Accessed 18 Sept 2019

Baek SG, Magda JJ (2003) Monolithic rheometer plate fabricated using silicon micromachining technology and containing miniature pressure sensors for N1 and N2 measurements. J Rheol 47(5):1249–1260. https://doi.org/10.1122/1.1595095

Barnes HA, Hutton JF, Walters K (1989) An introduction to rheology (Vol. 3). Elsevier Science, New York, p 8–59

Berret JF (2006) Rheology of wormlike micelles: equilibrium properties and shear banding transitions. Molecular Gels: Materials with Self-Assembled Fibrillar Networks, 667–720. https://doi.org/10.1007/1-4020-3689-2_20/COVER

Casanellas L, Alves MA, Poole RJ, Lerouge S, Lindner A (2016) The stabilizing effect of shear thinning on the onset of purely elastic instabilities in serpentine microflows. Soft Matter 12(29):6167–6175. https://doi.org/10.1039/c6sm00326e

Chen L, McDonald TO, Adams DJ (2013) Salt-induced hydrogels from functionalised-dipeptides. *RSC*. Advances 3(23):8714–8720. https://doi.org/10.1039/c3ra40938d

Chen L, Morris K, Laybourn A, Elias D, Hicks MR, Rodger A, Serpell L, Adams DJ (2010) Self-assembly mechanism for a naphthalene-dipeptide leading to hydrogelation. Langmuir 26(7):5232–5242. https://doi.org/10.1021/la903694a

Divoux T, Fardin MA, Manneville S, Lerouge S (2016) Shear banding of complex fluids. Annu Rev Fluid Mech 48:81–103. https://doi.org/10.1146/annurev-fluid-122414-034416

Draper ER, Dietrich B, McAulay K, Brasnett C, Abdizadeh H, Patmanidis I, Marrink SJ, Su H, Cui H, Schweins R, Seddon A, Adams DJ (2020) Using small-angle scattering and contrast matching to understand molecular packing in low molecular weight gels. Matter 2(3):764–778. https://doi.org/10.1016/J.MATT.2019.12.028

Draper ER, Su H, Brasnett C, Poole RJ, Rogers S, Cui H, Seddon A, Adams DJ (2017a) Opening a Can of Worm(-like Micelle)s: The effect of temperature of solutions of functionalized dipeptides. Angewandte Chemie - International Edition 56(35):10467–10470. https://doi.org/10.1002/anie.201705604

Draper ER, Wallace M, Schweins R, Poole RJ, Adams DJ (2017b) Nonlinear effects in multicomponent supramolecular hydrogels. Langmuir 33(9):2387–2395. https://doi.org/10.1021/acs.langmuir.7b00326

Du X, Zhou J, Shi J, Xu B (2015) Supramolecular hydrogelators and hydrogels: from soft matter to molecular biomaterials. Chem Rev 115(24):13165–13307. https://doi.org/10.1021/ACS.CHEMREV.5B00299

Fardin MA, Lerouge S (2012) Instabilities in wormlike micelle systems: from shear-banding to elastic turbulence. Eur Physical J E 35(9):91. https://doi.org/10.1140/epje/i2012-12091-0

Fardin MA, Lerouge S (2014) Flows of living polymer fluids. Soft Matter 10(44):8789–8799. https://doi.org/10.1039/c4sm01148a

Fischer P, Rehage H (1997) Non-linear flow properties of viscoelastic surfactant solutions. Rheol Acta 36(1):13–27. https://doi.org/10.1007/BF00366720

García-Sandoval JP, del Campo AM, Bautista F, Manero O, Puig JE (2018) Nonhomogeneous flow of micellar solutions: a kinetic—network theory approach. AIChE J 64(6):2277–2292. https://doi.org/10.1002/AIC.16079

Gaudino D, Costanzo S, Ianniruberto G, Grizzuti N, Pasquino R (2020) Linear wormlike micelles behave similarly to entangled linear polymers in fast shear flows. J Rheol 64(4):879. https://doi.org/10.1122/8.0000003

Giesekus H (1982) A simple constitutive equation for polymer fluids based on the concept of deformation-dependent tensorial mobility. J Nonnewton Fluid Mech 11(1–2):69–109. https://doi.org/10.1016/0377-0257(82)85016-7

Helgeson ME, Reichert MD, Hu YT, Wagner NJ (2009) Relating shear banding, structure, and phase behavior in wormlike micellar solutions. Soft Matter 5(20):3858–3869. https://doi.org/10.1039/b900948e

Kim S, Mewis J, Clasen C, Vermant J (2013) Superposition rheometry of a wormlike micellar fluid. Rheol Acta 52(8–9):727–740. https://doi.org/10.1007/s00397-013-0718-2

Larson RG (1997) The elastic stress in "film fluids." J Rheol 41(2):365–372. https://doi.org/10.1122/1.550857

Lee J-Y, Magda JJ, Hu H, Larson RG (2002) Cone angle effects, radial pressure profile, and second normal stress difference for shear-thickening wormlike micelles. J Rheol 46:1693. https://doi.org/10.1122/1.1428319

Lerouge S, Berret J-F (2009) Shear-induced transitions and instabilities in surfactant wormlike micelles. Adv Polym Sci 230:1–71. Springer, Berlin, Heidelberg. https://doi.org/10.1007/12_2009_13

López-Barrón CR, Gurnon AK, Eberle APR, Porcar L, Wagner NJ (2014) Microstructural evolution of a model, shear-banding micellar solution during shear startup and cessation. Phys Rev E 89(4):042301. https://doi.org/10.1103/PhysRevE.89.042301

Maklad O, Poole RJ (2021) A review of the second normal-stress difference; its importance in various flows, measurement techniques, results for various complex fluids and theoretical predictions. J Non-Newton Fluid Mech 292:104522. Elsevier. https://doi.org/10.1016/j.jnnfm.2021.104522

McAulay K, Ucha PA, Wang H, Fuentes-Caparrós AM, Thomson L, Maklad O, Khunti N, Cowieson N, Wallace M, Cui H, Poole RJ, Seddon A, Adams DJ (2020) Controlling the properties of the micellar and gel phase by varying the counterion in functionalised-dipeptide systems. Chem Commun 56(29):4094–4097. https://doi.org/10.1039/d0cc01252a

Morozov AN, van Saarloos W (2007) An introductory essay on subcritical instabilities and the transition to turbulence in visco-elastic

parallel shear flows. Phys Rep 447(3–6):112–143. https://doi.org/10.1016/J.PHYSREP.2007.03.004

Ober TJ (2013) Role of viscoelasticity and non-linear rheology in flows of complex fluids at high deformation rates (Doctoral dissertation, Massachusetts Institute of Technology). https://dspace.mit.edu/handle/1721.1/85532. Accessed 19 Oct 2021

Oelschlaeger C, Schopferer M, Scheffold F, Willenbacher N (2009) Linear-to-branched micelles transition: a rheometry and diffusing wave spectroscopy(DWS) study. Langmuir 25(2):716–723. https://doi.org/10.1021/LA802323X/ASSET/IMAGES/MEDIUM/LA-2008-02323X_0009.GIF

Phan-Thien N, Tanner RI (1977) A new constitutive equation derived from network theory. J Nonnewton Fluid Mech 2(4):353–365. https://doi.org/10.1016/0377-0257(77)80021-9

Pipe CJ, Kim NJ, Vasquez PA, Cook LP, McKinley GH (2010) Wormlike micellar solutions: II. Comparison between experimental data and scission model predictions. J Rheol 54(4):881–913

Poole RJ (2012) The Deborah and Weissenberg numbers. Rheol Bull 53(2):32–39. http://www.smp.uq.edu.au/pitch. Accessed 28 July 2021

Poole RJ (2016) Measuring normal-stresses in torsional rheometers : a practical guide. Bri Soc Rheol, Rheol Bull 57(2):36–46

Rehage H, Hoffmann H (1988) Rheological properties of viscoelastic surfactant systems. J Phys Chem 92(16):4712–4719. https://doi.org/10.1021/j100327a031

Rehage H, Hoffmann H (1991) Viscoelastic surfactant solutions: model systems for rheological research. Mol Phys 74(5):933–973. https://doi.org/10.1080/00268979100102721

Rothstein JP, Mohammadigoushki H (2020) Complex flows of viscoelastic wormlike micelle solutions. J Non-Newtonian Fluid Mech 285:104382. https://doi.org/10.1016/j.jnnfm.2020.104382

Vilageliu LC (2013) Oscillatory pipe flow of wormlike micellar solutions. http://diposit.ub.edu/dspace/handle/2445/35516. Accessed 15 Aug 2021